International Journal of Refrigeration 140 (2022) 57–69

Contents lists available at ScienceDirect

International Journal of Refrigeration

journal homepage: www.elsevier.com/locate/ijrefrig

General heat transfer correlations for supercritical carbon dioxide heated in vertical tubes for upward and downward flows

Corrélations générales de transfert de chaleur pour le dioxyde de carbone supercritique chauffé dans des tubes verticaux pour des écoulements ascendants et descendants

Zuliang Ye [a,b], Alireza Zendehboudi [b,*], Armin Hafner [b], Feng Cao [a,*]

[a] School of Energy and Power Engineering, Xi'an Jiaotong University, 28 Xianning West Road, 710049, Xi'an, China
[b] Department of Energy and Process Engineering, Norwegian University of Science and Technology (NTNU), Kolbjørn Hejes v 1B, 7491 Trondheim, Norway

ARTICLE INFO

Keywords:
Supercritical carbon dioxide
Heat transfer
General correlation
Vertical flow
Genetic programming
Mots clés:
Transfert de chaleur
Dioxyde de carbone supercritique
Corrélation générale
Écoulement vertical
État critique

ABSTRACT

Supercritical CO_2 is a promising working fluid for many industrial applications. To improve the performances of relevant components and systems, the prediction of the heat transfer of supercritical CO_2 is an important research topic. General explicit heat transfer correlations of supercritical CO_2 for upward and downward flows heated in circular tubes were established using the genetic programming (GP) method. A total of 12720 experimental data points from 22 publications were collected to develop the models. The data included hydraulic diameter from 0.0992 to 22 mm, bulk temperature from -6.0 to 134.5°C, pressure from 7.44 to 10.50 MPa, mass flux from 50 to 4834 kg•$(m^2•s)^{-1}$, heat flux from 2.9 to 748 kW•m^{-2} and wall temperature from 6.4 to 368.2°C. The database was divided into four parts according to the flow direction and the relationship between the bulk temperature and the pseudo-critical temperature. The developed correlations considered various non-dimensional parameters as the independent variables to reflect the effects of supercritical properties, flow acceleration and buoyancy on the heat transfer. The results showed that the proposed correlations had excellent accuracy with a mean absolute relative error (MARE) of 20.10% based on prediction with the iterated wall temperature. The developed correlations outperformed the existing correlations in the literature. Compared to other correlations, the trend analysis indicated that these newly developed correlations could appropriately present the physics sense when the condition parameters varied.

1. Introduction

Carbon dioxide (CO_2) has many attractive characteristics, including non-toxicity, incombustibility, safety, low cost and environmental friendliness, and is widely used in refrigeration, air conditioning, heat pump systems and a variety of industrial applications (Ehsan et al., 2018). CO_2 has a low critical temperature of 31.1°C and high critical pressure of 7.38 MPa, and thus the heat transfer on the high-pressure side of a CO_2 cycle, such as the CO_2 Rankine cycle (Zhang et al., 2019), is usually a supercritical process with temperature change. Due to the significant changes in the physical characteristics of CO_2 near the pseudo-critical temperature, heat transfer at a supercritical pressure significantly differs from that at a subcritical pressure (Zendehboudi et al., 2021). During the heat transfer of supercritical CO_2 (SCO_2), the temperature change occurs near the wall and the properties in the boundary layer accordingly vary, which essentially affects the heat transfer (Bae et al., 2010). Therefore, to optimize the performances of components associated with SCO_2 and further the system efficiency, it is important to investigate and predict the heat transfer of SCO_2.

The heat transfer of SCO_2 has been extensively researched and reviewed, which is valuable to provide a knowledge base. Cheng et al. (2008) comprehensively analyzed the experimental data and correlations for SCO_2 cooled in macro/micro-channels. Rao et al. (2016) reviewed the factors influencing the heat transfer of SCO_2, including tube diameter, channel characteristics, heat flux, mass flux, inlet pressure and inlet temperature. Cabeza et al. (2017) reviewed and presented the experimental studies and correlations for horizontal tubes, vertical tubes, inclined tubes, closed-loop circular pipes and mini-channels. Ehsan et al. (2018) discussed possible reasons for heat transfer

* Corresponding authors.
E-mail addresses: alireza.zendehboudi@ntnu.no (A. Zendehboudi), fcao@mail.xjtu.edu.cn (F. Cao).

https://doi.org/10.1016/j.ijrefrig.2022.05.013
Received 27 December 2021; Received in revised form 27 April 2022; Accepted 14 May 2022
Available online 18 May 2022

Nomenclature

Symbols

Ac	Flow acceleration parameter [-]
B	Buoyancy parameter from Kim et al. [-]
Bu	Buoyancy parameter [-]
c_p	Isobaric specific heat [kJ•(kg•K)$^{-1}$]
$\overline{c}_p$	Average isobaric specific heat [kJ•(kg•K)$^{-1}$]
D	Diameter [mm]
g	Gravitational acceleration [m•s^{-2}]
G	Mass flux [kg•(m^2•s)$^{-1}$]
$\overline{Gr}$	Average Grashof number [-]
Gr_q	Grashof number based on heat flux [-]
h	Enthalpy [kJ•kg^{-1}]
k	Thermal conductivity [W•(m•K)$^{-1}$]
K	Non-dimensional parameter representing evaporation induced momentum force relative to inertia force [-]
L	Length [m]
n	Exponent [-]
N	Number of data points [-]
Nu	Nusselt number [-]
$\overline{Nu}$	Average Nusselt number [-]
p	Pressure [MPa]
q	Heat flux [kW•m^{-2}]
q^+	Non-dimensional heat flux [-]
Re	Reynolds number [-]
Pr	Prandtl number [-]
$\overline{Pr}$	Average Prandtl number [-]
R^2	Coefficient of determination [-]
T	Temperature [°C]
β	Volume expansion coefficient [K^{-1}]
μ	Dynamic viscosity [Pa•s]
ν	Kinematic viscosity [m^2•s^{-1}]
ρ	Density [kg•m^{-3}]
$\overline{\rho}$	Average density [kg•m^{-3}]
τ	Shear stress [N•m^{-2}]

Abbreviations

ANN	Artificial neural network
ARE	Absolute relative error
GP	Genetic programming
HTC	Heat transfer coefficient
HTD	Heat transfer deterioration
MARE	Mean absolute relative error
SCO_2	Supercritical carbon dioxide

Subscripts

b	Bulk
BFL	Buffer layer
cal	Calculated
exp	Experimental
h	Hydraulic
pc	Pseudo-critical
VSL	Viscous sub-layer
w	Wall

deterioration (HTD) and reviewed the characteristics of pressure drop, convective heat transfer behavior, wall temperature distribution and influence of buoyancy. Xie et al. (2020) conducted a review focusing on the HTD of SCO_2 in vertical tubes. They analyzed the influences of the boundary conditions on the HTD and assessed the identification methods to distinguish the HTD.

Regarding the SCO_2 heated in vertical tubes, a lot of experimental studies have been published. Song et al. (2008) conducted experiments at different diameters and found that L/D and q_w/G could be used as the criteria for the similarity of heat transfer. In addition, they also suggested that the heat transfer at a larger diameter was more susceptible to decrease due to the buoyancy. Kim and Kim (2011a) stated that the flow acceleration predominantly affected the heat transfer in their experimental range. Liu et al. (2017) made efforts to improve the non-dimensional parameters for buoyancy and flow acceleration and theoretically established thresholds of them, which was validated against experimental data. Zhang et al. (2018) focused on heat transfer at low mass flux. They found that the heat transfer at lower mass flux did not deteriorate but rather enhanced, which mainly resulted from the combined effects of strong buoyancy and high specific heat.

Furthermore, based on the experimental data, plenty of correlations have been developed (Bae et al., 2010; Fan et al., 2019; Gupta et al., 2013a; Jackson, 2013; Jackson and Hall, 1979; Kim and Kim, 2011a; Kim and Kim, 2010, 2011b; Kim et al., 2008; Li et al., 2010; Liao and Zhao, 2002; Liu et al., 2017; Saltanov et al., 2015; Zhang et al., 2018). The concept of developing the general heat transfer model from a large database has also been put forward. Zhu et al. (2020) created a new non-dimensional parameter that represented evaporation induced momentum force relative to inertia force, and developed a general correlation based on 5560 data points of supercritical CO_2, water and R134a. Ye et al. (2019) and Sun et al. (2021) both built the experimental databases and applied the artificial neural network (ANN) to model the heat transfer of SCO_2.

Most available empirical correlations for predicting SCO_2 heat transfer were developed for specific conditions and there were deviations between each other. Besides, although the ANN model can predict the SCO_2 heat transfer with acceptable accuracy, it was not convenient to use for others. Therefore, well-verified general correlations were required to fulfill the demand. In this paper, 12720 data points from 22 publications were collected to develop correlations that were applicable for upward and downward vertical SCO_2 flow regimes. The genetic programming was used to develop explicit correlations without an initial prediction model, which was easier to use for others than black-box algorithms like ANN. Based on the experimental database that covered a wide range of parameters, a comprehensive comparison between the proposed correlations and some existing correlations from the literature was performed. The accuracies of the correlations were evaluated and shown in detail. In addition, detailed trend analyses were performed.

2. Materials and method

2.1. Genetic programming

In the current study, the genetic programming (GP) was used to develop heat transfer general correlations for SCO_2 upward and downward flows heated in circular tubes. The GP method can create explicit equations without utilizing initial prediction models, which gives it an inherent advantage over traditional mathematical and statistical methods as well as black-box algorithms like ANN (Sadat Hosseini et al., 2021). The genetic programming was coded in Python using the GPlearn package. Fig. 1 is the flow chart of the genetic programming.

To begin, the dimensionless input parameters were inserted and the specific parameters of the genetic programming model were set. The population size was set at 3000, with a maximum of 1000 evolution generations. In the selection procedure, a tournament selection type with a size of 3 was used. The crossover and mutation rates were set to 70% and 25%, respectively.

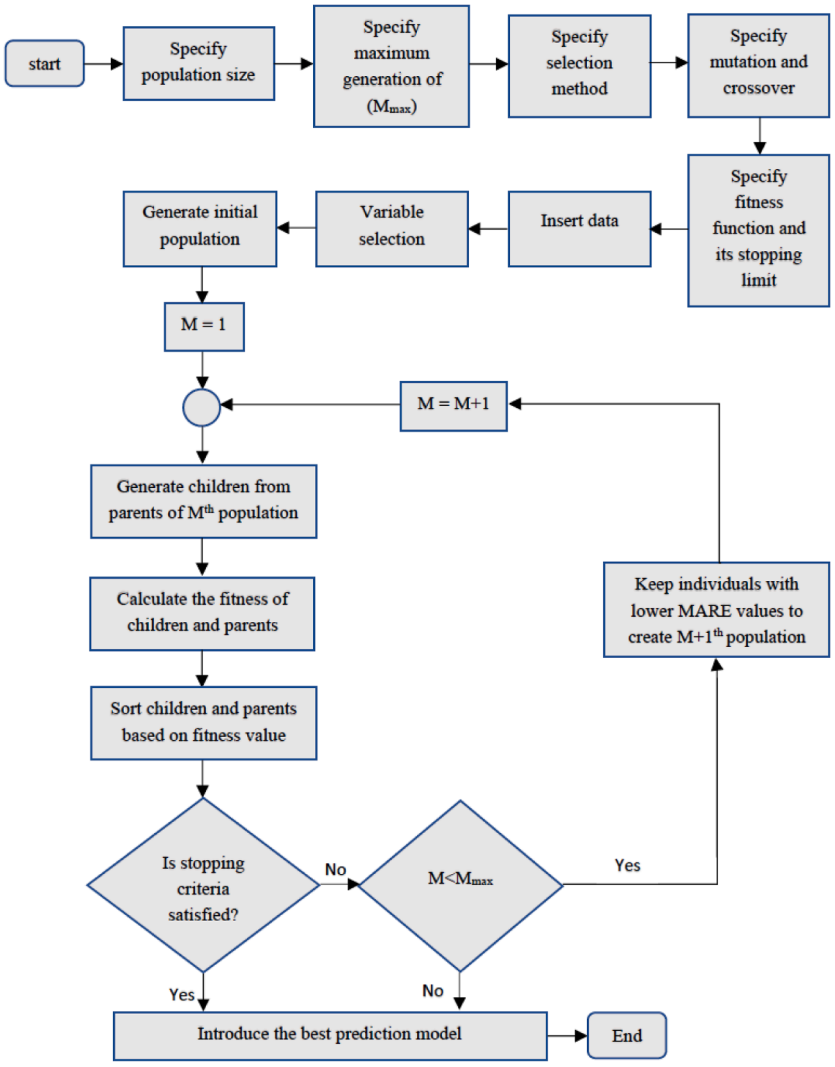

Fig. 1. Flow chart of the genetic programming.

A variable selection method was developed to eliminate the non-informative parameters to obtain a more accurate result with a less complex model. After determining the most influential input parameters from the initial input parameters, the program created an initial population. At this point, the algorithm randomly created the initial generation of a population including n individuals to describe the relationship between the input and output variables. Each individual was an equation to predict the Nusselt number of SCO_2 including simple arithmetic operations (+, -, *, /), geometric operators (sin, cos, tan) and exponential operators (^, sqrt, e^x, log, ln). The first created generation became the parent generation. The fitness of each individual was evaluated and checked using the mean absolute relative error (MARE). At each iteration, the genetic operators, such as selection, crossover and mutation were applied to the individuals of the population. In the next step, the individuals with relatively low MARE values were selected using the tournament selection method, and the crossover and mutation were performed to create the first children generation. The crossover was the process of combining the genetic information of two parents to create the new children, while parts of the children were randomly modified by the mutation operator (Jamei et al., 2021). In the following stage, the MARE of children was evaluated to see if any newly developed correlation satisfied the termination condition. The steps from evaluation to mutation continued until the number of iterations reached the maximum evolution generations or satisfied the termination requirement. Ultimately, the GP algorithm returned the best solution.

2.2. *Experimental database*

Based on 22 publications about the SCO_2 heated in vertical circular tubes, an experimental database including 12720 data points was built. The data points were obtained from the figures in the selected publications utilizing the software GetData. During the data collection, the repetitive data points were recognized and removed. Table 1 summarizes the information on the database. The thermophysical properties of the SCO_2 were determined based on the NIST REFPROP 9.1 (Lemmon et al., 2013).

For developing the correlations, the independent variables should be determined first. Through the literature review, it can be found that the Reynolds number and Prandtl number were always used. Considering the variations of SCO_2 thermophysical properties during the heat transfer process, the property ratios between the wall and bulk temperatures were adopted, including density, viscosity, thermal conductivity and specific heat. Moreover, some publications considered the buoyancy force and flow acceleration because they affected the shear stress distributions in the turbulent boundary layer (Kim and Kim, 2011b). Given the information above, the heat transfer correlations in this study were developed as below:

Table 1
Source publications and parameter ranges of the experimental database.

Reference	D_h [mm]	T_b [°C]	h_b [kJ•kg^{-1}]	p [MPa]	G [kg•(m^2•s)$^{-1}$]	q_w [kW•m^{-2}]	T_w [°C]	Flow direction	Number of points
Kim et al. (2007)	4.4	27.3-109.3	271.3-533.8	7.75-8.85	400-1200	20-150	31.0-147.6	Upward	1036
Song et al. (2008)	4.4, 9	6.8-93.3	212.1-509.8	8.12	400-1200	30-50	22.3-124.5	Upward	331
Jiang et al. (2008)	0.27	25.3-75.1	261.6-477.6	8.6	2691.3-2716.9	92.2-549.0	29.4-155.1	Upward & Downward	196
Cho et al. (2009)	2, 4.4	21.1-64.4	249.9-464.7	8.12	1200	50-130	30.9-97.7	Upward	75
Bae et al. (2010)	6.32	10.0-78.8	220.0-488.7	7.75-8.12	285-1200	29.3-70	20.3-140.4	Upward	1263
Li et al. (2010)	2	24.8-41.1	259.4-370.2	8.8	314.74	6.5-52.0	28.2-145.8	Upward & Downward	462
Kim and Kim (2010)	4.5	29.1-36.6	276.9-344.5	8.34	663	62	41.3-47.8	Upward	20
Kim and Kim (2011a)	4.5	28.6-76.7	277.4-475.0	7.44-9.09	233-873	52.8-216.2	49.2-193.2	Upward & Downward	140
Bae et al. (2011)	6.32	14.7-89.6	232.6-507.7	7.75	400	30-50	31.3-146.5	Upward	184
Kim and Kim (2011b)	4.5	31.9-114.5	287.5-536.0	8.42-8.56	230-610	82.6-190.1	62.5-238.5	Upward	60
Gupta et al. (2013b)	8.06	31.0-34.9	285.2-311.9	8.38	784	18.4	37.2-45.6	Upward	22
Jiang et al. (2013)	0.0992	23.0-134.5	253.9-565.2	7.68-8.68	1823-4834	85-748	26.2-182.8	Downward	94
Zahlan et al. (2015)	8, 22	7.5-63.9	213.9-460.0	7.52-8.56	200-2000	5.1-436	13.6-191.3	Upward	1799
Jiang (2015)	8	8.6-52.0	216.2-434.8	7.66-8.53	402-1999	25-350	17.6-201.4	Upward	1293
Liu et al. (2016)	5.98	16.7-105.4	236.0-526.2	8.12-8.9	337.2-479.2	39.4-70.9	40.7-169.5	Upward	130
Lei et al. (2017)	5	4.7-93.7	207.8-511.3	7.5-8	100-200	8.96-56	25.5-368.2	Upward	527
Liu et al. (2017)	10	16.0-43.0	236.6-426.1	7.45-7.61	303.5-901.8	121.8-256.2	55.7-297.9	Upward & Downward	66
Xu et al. (2017)	0.953	22.6-48.0	250.7-389.6	9.5	255	12-63	29.0-182.2	Upward & Downward	981
Eter et al. (2017)	8	9.5-97.0	219.1-513.1	7.60-8.56	192-1184	2.9-126.3	17.5-223.7	Upward	2215
Zhang et al. (2018)	16	-6.0-105.3	183.5-508.2	7.5-10.5	100-500	5-50	6.4-226.4	Upward	736
Lei et al. (2019)	5	3.8-89.5	204.4-482.7	7.5-10.5	50-200	5-100	11.9-308.7	Upward	997
Zhang et al. (2020)	4	17.8-67.0	238.6-470.8	7.5-9	90-321	12.7-32.5	33.4-157.8	Upward	93
Total	0.0992-22	-6.0-134.5	183.5-565.2	7.44-10.50	50-4833	2.9-748	6.4-368.2		12720

$$Nu_b = f\left(\mathrm{Re}_b, \overline{\mathrm{Pr}}, \frac{\rho_w}{\rho_b}, \frac{\mu_w}{\mu_b}, \frac{k_w}{k_b}, \frac{\overline{c}_p}{c_{p,b}}, Bu, q^+\right) \tag{1}$$

where Nu_b is the Nusselt number; Re_b is the Reynolds number at bulk temperature; $\overline{\mathrm{Pr}}$ is the average Prandtl number; ρ_b, μ_b, k_b and $c_{p,b}$ are the density, dynamic viscosity, thermal conductivity and isobaric specific heat at bulk temperature, and ρ_w, μ_w and k_w are the properties at wall temperature; $\overline{c}_p$ is the average isobaric specific between the bulk and wall temperatures; Bu is the buoyancy parameter; q^+ is the non-dimensional heat flux. The Re_b can be expressed as:

$$\mathrm{Re}_b = \frac{GD_h}{\mu_b} \tag{2}$$

where G is the mass flux; D_h is the hydraulic diameter. The $\overline{\mathrm{Pr}}$ can be expressed as:

$$\overline{\mathrm{Pr}} = \frac{\mu_b \overline{c}_p}{k_b} \tag{3}$$

where $\overline{c}_p$ can be defined as:

$$\overline{c}_p = \frac{h_w - h_b}{T_w - T_b} \tag{4}$$

where h_b and h_w are the enthalpy at bulk and wall temperatures (T_b and T_w), respectively. To represent the effect of flow acceleration on the heat transfer, the q^+ can be defined as (Kim and Kim, 2011a):

$$q^+ = \frac{q_w \beta_b}{G c_{p,b}} \tag{5}$$

where q_w is the heat flux at wall; β_b is the volume expansion coefficient. The Bu can be expressed as:

Table 2
The ranges of the independent variables for developing correlations.

Conditions	Re_b	$\overline{\mathrm{Pr}}$	ρ_w/ρ_b	μ_w/μ_b	k_w/k_b	$\overline{c}_p/c_{p,b}$	Bu	q^+
Upward, $T_b > T_{pc}$	6841-7.45 × 10^5	0.41-7.72	0.18-0.92	0.60-1.48	0.19-1.65	1.74 × 10^{-2}-0.96	2.34 × 10^{-9}-3.85 × 10^{-3}	1.83 × 10^{-4}-4.75 × 10^{-3}
Upward, $T_b \le T_{pc}$	2499-4.68 × 10^5	0.41-22.46	0.12-0.97	0.18-0.94	0.17-1.64	1.08 × 10^{-2}-4.17	1.45 × 10^{-8}-1.03 × 10^{-2}	4.44 × 10^{-5}-4.75 × 10^{-3}
Downward, $T_b > T_{pc}$	6086-2.32 × 10^5	0.40-2.75	0.25-0.85	0.60-1.10	0.22-1.11	1.32 × 10^{-2}-0.97	5.67 × 10^{-10}-3.44 × 10^{-5}	6.27 × 10^{-4}-3.46 × 10^{-3}
Downward, $T_b \le T_{pc}$	2827-1.98 × 10^5	0.37-21.56	0.14-0.96	0.26-0.93	0.14-1.12	5.44 × 10^{-3}-3.43	1.02 × 10^{-9}-3.38 × 10^{-4}	8.25 × 10^{-5}-3.61 × 10^{-3}

Table 3
Correlations used for the comparison.

Author	Correlations	Application range
Dittus and Boelter (1985)	$Nu_b = 0.023\mathrm{Re}_b^{0.8}\mathrm{Pr}_b^{0.4}$	Subcritical single-phase
Jackson and Hall (1979)	$Nu_b = 0.0183\mathrm{Re}_b^{0.82}\mathrm{Pr}_b^{0.5}\left(\frac{\rho_w}{\rho_b}\right)^{0.3}\left(\frac{\bar{c}_p}{c_{p,b}}\right)^{n}$ $n=\begin{cases}0.4, \text{for}\ \frac{T_b}{T_{pc}}<\frac{T_w}{T_{pc}}\le 1 \text{or} 1.2\le\frac{T_b}{T_{pc}}<\frac{T_w}{T_{pc}}\\ 0.4+0.2\left(\frac{T_w}{T_{pc}}-1\right), \text{for}\ \frac{T_b}{T_{pc}}\le 1<\frac{T_w}{T_{pc}}\\ 0.4+0.2\left(\frac{T_w}{T_{pc}}-1\right)\left[1-5\left(\frac{T_b}{T_{pc}}-1\right)\right], \text{for} 1<\frac{T_b}{T_{pc}}<1.2 \text{and}\ \frac{T_b}{T_{pc}}<\frac{T_w}{T_{pc}}\end{cases}$ T is in Kelvin.	Not available
Jackson (2013)	$Nu_b = 0.0183\mathrm{Re}_b^{0.82}\overline{\mathrm{Pr}}^{0.5}\left(\frac{\rho_w}{\rho_b}\right)^{0.3}$	Not available
Liao and Zhao (2002)	$Nu = 0.354\mathrm{Re}_b^{0.8}\mathrm{Pr}_b^{0.4}Bu^{0.157}\left(\frac{\rho_w}{\rho_b}\right)^{1.297}\left(\frac{\bar{c}_p}{c_{p,b}}\right)^{0.296}$, upwardflow $Nu = 0.643\mathrm{Re}_b^{0.8}\mathrm{Pr}_b^{0.4}Bu^{0.186}\left(\frac{\rho_w}{\rho_b}\right)^{2.154}\left(\frac{\bar{c}_p}{c_{p,b}}\right)^{0.751}$, downwardflow	D_h: 0.7-2.16 mm p: 7.4-12 MPa T_b: 20-110°C T_w-T_b: 2-30°C m: 0.02-0.2 kg•min^{-1} $\overline{Gr}/\mathrm{Re}_b^{2.7}$:2 × 10^{-9}-10^{-5}
Kim and Kim (2011a)	$Nu_b = 2.0514\mathrm{Re}_b^{0.928}\mathrm{Pr}_b^{0.742}\left(\frac{\rho_w}{\rho_b}\right)^{1.305}\left(\frac{\mu_w}{\mu_b}\right)^{-0.669}\left(\frac{\bar{c}_p}{c_{p,b}}\right)^{0.888}(q^+)^{0.792}$	D_h: 4.5 mm p: 7.46-10.26 MPa T_b: 29-115°C G: 208-874 kg•(m^2•s)$^{-1}$ q_w: 38-234 kW•m^{-2}
Kim and Kim (2010)	$Nu_b = 0.226\mathrm{Re}_b^{1.174}\mathrm{Pr}_b^{1.057}\left(\frac{\rho_w}{\rho_b}\right)^{0.571}\left(\frac{\bar{c}_p}{c_{p,b}}\right)^{1.032}Ac^{0.489}Bu_K^{0.0021}$ $Ac = \frac{q^+}{\mathrm{Re}_b^{0.625}}\left(\frac{\mu_w}{\mu_b}\right)\left(\frac{\rho_b}{\rho_w}\right)^{0.5}$ $Bu_K = \frac{Gr_q}{\mathrm{Re}_b^{3.425}\overline{\mathrm{Pr}}_b^{0.8}}\left(\frac{\mu_w}{\mu_b}\right)\left(\frac{\rho_b}{\rho_w}\right)^{0.5}$ $Gr_q = \frac{g\beta_b D_h^4 q_w}{\nu_b^2 k_b}$	D_h: 4.5 mm p: 7.46-10.26 MPa T_b: 29-115°C G: 208-874 kg•(m^2•s)$^{-1}$ q_w: 38-234 kW•m^{-2}
Kim and Kim (2011b)	$\frac{1}{Nu} = \frac{1}{Nu_{VSL}} + \frac{1}{Nu_{BFL}}$ $\frac{1}{Nu_{VSL}} = \frac{0.00249\mu_b}{D_h\sqrt{\rho_b\tau_w}}\left(\frac{\rho_w}{\rho_b}\right)^{-3.461}\left(\frac{\mu_w}{\mu_b}\right)^{3.357}\mathrm{Re}_b^{-0.412}(q^+)^{-1.621}$ $\frac{1}{Nu_{BFL}} = \frac{1}{0.192\mathrm{Re}_b^{0.625}\mathrm{Pr}_b^{0.597}\left(\frac{\bar{c}_p}{c_{p,b}}\right)^{0.826}}$	D_h: 4.5 mm p: 7.46-10.26 MPa T_b: 29-115°C G: 208-874 kg•(m^2•s)$^{-1}$ q_w: 38-234 kW•m^{-2}
Gupta et al. (2013a)	$Nu_b = 0.01\mathrm{Re}_b^{0.89}\overline{\mathrm{Pr}}^{-0.14}\left(\frac{\rho_w}{\rho_b}\right)^{0.93}\left(\frac{k_w}{k_b}\right)^{0.22}\left(\frac{\mu_w}{\mu_b}\right)^{-1.13}$	D_h: 8 mm p: 7.57-8.8 MPa T_{in}: 20-40°C G:706-3169 kg•(m^2•s)$^{-1}$ q_w: 9.3-616.6 kW•m^{-2}
Saltanov et al. (2015)	$Nu_b = 0.0331\mathrm{Re}_b^{0.784}\overline{\mathrm{Pr}}^{0.444}\left(\frac{\rho_w}{\rho_b}\right)^{0.640}$	D_h: 4.4-8.1 mm p: 7.57-8.91 MPa T_b: 5-161°C G:199-3048 kg•(m^2•s)$^{-1}$ q_w: 9.9-616 kW•m^{-2}
Zhang et al. (2018)	$Nu_b = \begin{cases}0.00672\mathrm{Re}_b^{1.414}\overline{\mathrm{Pr}}^{-0.005}\left(\frac{\rho_w}{\rho_b}\right)^{0.448}\left(\frac{\bar{c}_p}{c_{p,b}}\right)^{0.218}Bu^{0.586}, \mathrm{h}_b < 0.9h_{pc}\\ 0.056\mathrm{Re}_b^{0.829}\overline{\mathrm{Pr}}^{0.35}\left(\frac{\rho_w}{\rho_b}\right)^{-0.095}\left(\frac{\bar{c}_p}{c_{p,b}}\right)^{0.214}Bu^{0.142}, \mathrm{h}_b \ge 0.9h_{pc}\end{cases}$	D_h: 16 mm p: 7.5-10.5 MPa G: 50-200 kg•(m^2•s)$^{-1}$ q_w: 5-60 kW•m^{-2}
Zhu et al. (2020)	$Nu = 0.0012\mathrm{Re}_b^{0.9484}\overline{\mathrm{Pr}}^{0.718}K^{-0.0313}$ $K = \left(\frac{q_w}{G\cdot h_w}\right)^2\frac{\rho_b}{\rho_w}$	A general correlation for vertical upward supercritical flows
Kim et al. (2008)	$Nu_b = Nu_{Jackson\&Hall}f(B)$ $B = \frac{\overline{Gr}}{\mathrm{Re}_b^{2.7}\overline{\mathrm{Pr}}^{0.5}}$ $f(B) = \begin{cases}(0.8+6.0\times10^6B)^{-0.8}, \text{for} B\le 7.0\times10^{-8}\\ 0.261+3.068B^{0.1}, \text{for} 7.0\times10^{-8}<B\le 7.0\times10^{-7}\\ 1.47-6.7\times10^5B, \text{for} 7.0\times10^{-7}<B\le 1.0\times10^{-6}\\ 0.8, \text{for} 1.0\times10^{-6}<B\le 1.0\times10^{-5}\\ 0.1423B^{-0.15}, \text{for} B>1.0\times10^{-5}\end{cases}$	D_h: 2 mm p: 7.75-8.12 MPa T_{in}: 0-37°C G:400-1200 kg•(m^2•s)$^{-1}$ q_w: Up to 150 kW•m^{-2}

$$Bu = \frac{\overline{Gr}}{\mathrm{Re}_b^{2.7}} \tag{6}$$

where $\overline{Gr}$ is the average Grashof number and can be defined as:

$$\overline{Gr} = \frac{(\rho_b - \overline{\rho})\rho_b g D_h^3}{\mu_b^2} \tag{7}$$

where g is the gravitational acceleration; $\overline{\rho}$ is the average density between the wall and bulk temperatures and can be defined as:

$$\overline{\rho} = \frac{\int_{T_b}^{T_w} \rho dT}{T_w - T_b} \tag{8}$$

The ranges of the independent variables were calculated and summarized in Table 2. Because of the significant change of SCO_2 properties near the pseudo-critical point, to improve the accuracies of proposed correlations, the data points for upward and downward flows were divided based on the relationship between the bulk temperature T_b and the pseudo-critical temperature T_{pc}.

3. Results and discussion

3.1. General heat transfer correlations

According to experimental data, there existed nonlinear relations between the Nusselt number of SCO_2 and affecting parameters during the upward and downward flows heated in circular tubes. In this study, the proposed general correlations based on the GP method are as follows:

For upward flows and $T_b > T_{pc}$:

$$Nu_b = \mathrm{Re}_b Bu + \frac{0.143\left(\frac{\rho_w}{\rho_b}\right)\mathrm{Re}_b\overline{\mathrm{Pr}}}{(q^+)^{-0.603}} + \frac{\sqrt{\mathrm{Re}_b}\left(\frac{\rho_w}{\rho_b}\right)^2\left(0.423\overline{\mathrm{Pr}}\sqrt{\mathrm{Re}_b}\right)^{\frac{\rho_w}{\rho_b}}}{(q^+)^{-0.603}} \tag{9}$$

where the application ranges were: D_h: 0.27-16 mm; T_b: 31.7-114.5°C; p: 7.5-10.5 MPa; G: 50-2716.9 kg•(m^2•s)$^{-1}$; q_w: 5-549 kW•m^{-2}; T_w: 34.6-368.2°C.

For upward flows and $T_b \le T_{pc}$:

$$\begin{aligned} Nu_b = {} & 0.00123\mathrm{Re}_b\left(\frac{\rho_w}{\rho_b}\right) - 8.07\mathrm{Re}_b\left(\frac{\rho_w}{\rho_b}\right)\sin(q^+\overline{\mathrm{Pr}})^{1.21} - 0.137\mathrm{Re}_b q^+ \\ & + 1.7\mathrm{Re}_b q^+\left(\frac{\overline{c}_p}{c_{p,b}}\right)^{\frac{\rho_w}{\rho_b}+1} + 13.3\mathrm{Re}_b\sin(q^+\overline{\mathrm{Pr}})^{1.21}\tan\left(\tan\left(\frac{\rho_w}{\rho_b}\right)\right) \end{aligned} \tag{10}$$

where the application ranges were: D_h: 0.27-22 mm; T_b: -6.0-47.3°C; p: 7.5-10.5 MPa; G: 50-2716.9 kg•(m^2•s)$^{-1}$; q_w: 2.9-549 kW•m^{-2}; T_w: 6.4-297.9°C.

For downward flows and $T_b > T_{pc}$:

$$\begin{aligned} Nu_b = {} & 23.1\left(\frac{\overline{c}_p}{c_{p,b}}\right)^{\frac{\rho_w}{\rho_b}} + 5.97\cos(0.000241\mathrm{Re}_b) + 405\sqrt{\mathrm{Re}_b}q^+\overline{\mathrm{Pr}}\left(\frac{\rho_w}{\rho_b}\right)^2 \\ & + 0.00121\mathrm{Re}_b\overline{\mathrm{Pr}}Bu^{8.73e-5} - 8.01\overline{\mathrm{Pr}} - 9.61 \end{aligned} \tag{11}$$

where the application ranges were: D_h: 0.0992-10 mm; T_b: 31.4-134.5°C; p: 7.44-9.5 MPa; G: 233-4834 kg•(m^2•s)$^{-1}$; q_w: 48-748 kW•m^{-2}; T_w: 41.8-207.4°C.

For downward flows and $T_b \le T_{pc}$:

$$\begin{aligned} Nu_b = {} & 0.00115\mathrm{Re}_b\left(\frac{\overline{c}_p}{c_{p,b}}\right) + 56.8\mathrm{Re}_b\left(\frac{\overline{c}_p}{c_{p,b}}\right)^{\frac{\rho_w}{\rho_b}}\sin(q^+\overline{\mathrm{Pr}})^2 - 3.86\left(\frac{k_w}{k_b}\right) \\ & + 0.631\mathrm{Re}_b Bu^{-0.0534}\sin(q^+\overline{\mathrm{Pr}})\tan\left(1.56\left(\frac{\rho_w}{\rho_b}\right)\right) + 3.23 \end{aligned} \tag{12}$$

where the application ranges were: D_h: 0.0992-10 mm; T_b: 16.0-42.5°C; p: 7.44-9.5 MPa; G: 233-4834 kg•(m^2•s)$^{-1}$; q_w: 6.5-748 kW•m^{-2}; T_w: 24.0-142.1°C.

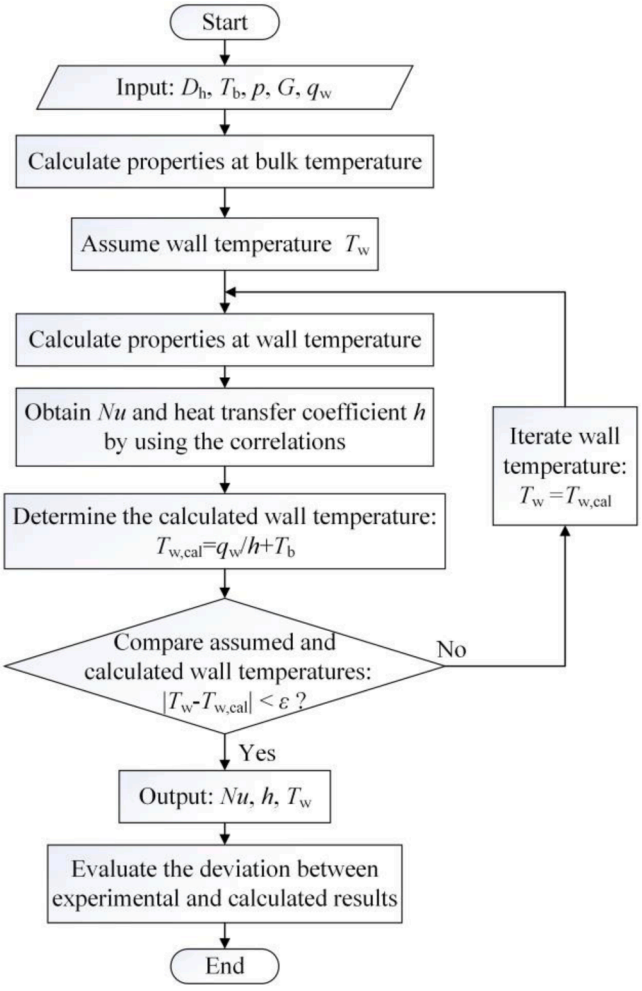

Fig. 2. Flow chart of the iterative method without inputting wall temperature (Zhu et al., 2020).

3.2. Assessment of the correlations

In this section, the accuracies of the proposed correlations and some existing correlations were assessed and compared. Table 3 shows the correlations used for the comparison, which covered different parameters and forms.

To evaluate the accuracies, the absolute relative error (ARE) of each data point was used:

$$ARE = \left|\frac{Nu_{cal} - Nu_{\mathrm{exp}}}{Nu_{\mathrm{exp}}}\right| \tag{13}$$

The mean absolute relative error (MARE) was defined as:

$$MARE = \frac{1}{N}\sum_{i=1}^{N}\left|\frac{Nu_{cal} - Nu_{\mathrm{exp}}}{Nu_{\mathrm{exp}}}\right| \tag{14}$$

The coefficient of determination (R^2) was adopted to assess the goodness of fit:

$$R^2 = \left[\frac{\sum_{i=1}^{N}\left(Nu_{\mathrm{exp},i} - \overline{Nu}_{\mathrm{exp}}\right)\left(Nu_{cal,i} - \overline{Nu}_{cal}\right)}{\sqrt{\sum_{i=1}^{N}\left(Nu_{\mathrm{exp},i} - \overline{Nu}_{\mathrm{exp}}\right)^2}\sqrt{\sum_{i=1}^{N}\left(Nu_{cal,i} - \overline{Nu}_{cal}\right)^2}}\right]^2 \tag{15}$$

Table 4
Summary of MARE and R^2 for different correlations.

Database	Assessment of correlations: MARE R^2													
Reference	Number of points	Dittus and Boelter (1985)	Jackson and Hall (1979)	Jackson (2013)	Liao and Zhao (2002)	Kim and Kim (2011a)	Kim and Kim (2010)	Kim and Kim (2011b)	Gupta et al. (2013a)	Saltanov et al. (2015)	Zhang et al. (2018)	Zhu et al. (2020)	Kim et al. (2008)	This study
Kim et al. (2007)	1036	58.92%	27.61%	22.02%	45.80%	36.62%	35.38%	55.57%	46.55%	22.33%	73.77%	37.76%	25.48%	17.61%
		0.20	0.75	0.88	0.19	0.60	0.69	0.00	0.21	0.77	0.07	0.79	0.71	0.64
Song et al. (2008)	331	68.85%	42.97%	40.85%	69.05%	47.48%	34.79%	48.43%	33.81%	23.39%	59.84%	39.59%	20.56%	18.01%
		0.59	0.90	0.94	0.33	0.76	0.85	0.23	0.57	0.87	0.12	0.92	0.94	0.43
Jiang et al. (2008)	196	37.37%	16.36%	13.36%	75.12%	38.98%	23.90%	58.04%	46.64%	23.76%	91.25%	41.42%	29.60%	47.73%
		0.01	0.35	0.56	0.11	0.35	0.65	0.00	0.08	0.06	0.01	0.34	0.16	0.21
Cho et al. (2009)	75	47.98%	24.12%	20.04%	36.79%	20.74%	40.21%	45.87%	36.75%	23.06%	76.64%	32.12%	20.24%	13.08%
		0.47	0.74	0.81	0.34	0.67	0.10	0.61	0.82	0.71	0.49	0.31	0.70	0.61
Bae et al. (2010)	1263	65.36%	36.51%	33.67%	56.23%	43.84%	36.40%	46.07%	32.20%	22.55%	60.53%	42.38%	20.86%	11.57%
		0.67	0.89	0.90	0.49	0.57	0.75	0.34	0.43	0.77	0.21	0.84	0.87	0.61
Li et al. (2010)	462	117.90%	102.58%	105.55%	259.35%	180.67%	76.21%	95.75%	39.73%	96.12%	88.29%	47.45%	49.47%	16.29%
		0.08	0.01	0.00	0.00	0.03	0.00	0.02	0.01	0.04	0.04	0.05	0.02	0.77
Kim and Kim (2010)	20	26.44%	9.93%	5.55%	29.69%	27.24%	21.10%	33.35%	60.99%	32.66%	73.27%	32.08%	31.07%	2.42%
		0.10	0.18	0.28	0.10	0.06	0.41	0.44	0.06	0.10	0.39	0.00	0.14	0.88
Kim and Kim (2011a)	140	182.14%	44.57%	26.97%	89.21%	46.35%	21.25%	17.03%	33.60%	26.45%	45.26%	43.92%	31.52%	19.60%
		0.07	0.49	0.68	0.00	0.66	0.67	0.63	0.58	0.54	0.35	0.74	0.55	0.84
Bae et al. (2011)	184	75.34%	39.13%	36.01%	67.10%	41.28%	33.49%	42.40%	25.97%	20.10%	53.46%	45.29%	14.76%	12.57%
		0.27	0.70	0.72	0.62	0.09	0.30	0.46	0.34	0.74	0.52	0.05	0.73	0.86
Kim and Kim (2011b)	60	131.68%	34.71%	29.21%	39.04%	69.45%	26.15%	25.08%	36.60%	23.86%	34.32%	45.59%	30.15%	20.00%
		0.01	0.26	0.35	0.03	0.34	0.28	0.08	0.31	0.40	0.09	0.36	0.34	0.85
Gupta et al. (2013b)	22	111.32%	178.40%	189.91%	224.33%	82.77%	128.84%	95.23%	14.01%	182.45%	76.90%	168.85%	172.29%	121.71%
		0.61	0.65	0.65	0.67	0.71	0.64	0.09	0.08	0.67	0.13	0.65	0.65	0.55
Jiang et al. (2013)	94	116.60%	70.70%	61.42%	87.84%	72.99%	58.34%	84.88%	48.39%	71.95%	84.31%	49.97%	89.31%	92.97%
		0.00	0.11	0.28	0.02	0.29	0.06	0.11	0.00	0.13	0.22	0.41	0.10	0.73
Zahlan et al. (2015)	1799	60.39%	30.96%	30.14%	88.62%	40.60%	60.81%	37.95%	31.84%	36.45%	53.02%	21.88%	33.11%	10.21%
		0.25	0.67	0.74	0.01	0.44	0.18	0.43	0.44	0.30	0.00	0.83	0.65	0.90
Jiang (2015)	1293	59.08%	30.10%	28.44%	78.55%	37.98%	59.82%	38.39%	35.26%	39.61%	79.08%	23.50%	26.28%	9.62%
		0.22	0.74	0.82	0.16	0.63	0.18	0.54	0.45	0.28	0.00	0.87	0.72	0.98
Liu et al. (2016)	130	96.27%	54.34%	50.19%	71.93%	73.59%	25.00%	25.05%	22.68%	25.08%	44.86%	32.66%	18.98%	10.34%
		0.29	0.53	0.56	0.48	0.11	0.46	0.36	0.53	0.68	0.40	0.09	0.67	0.85
Lei et al. (2017)	527	139.99%	44.85%	36.42%	225.87%	77.37%	55.15%	54.78%	60.15%	51.47%	32.81%	52.80%	76.55%	38.08%

(*continued on next page*)

Table 4 (*continued*)

Database	Assessment of correlations: MARE R^2	Dittus and Boelter (1985)	Jackson and Hall (1979)	Jackson (2013)	Liao and Zhao (2002)	Kim and Kim (2011a)	Kim and Kim (2010)	Kim and Kim (2011b)	Gupta et al. (2013a)	Saltanov et al. (2015)	Zhang et al. (2018)	Zhu et al. (2020)	Kim et al. (2008)	This study
Reference	Number of points													
Liu et al. (2017)	66	0.05	0.02	0.00	0.51	0.03	0.01	0.04	0.20	0.28	0.01	0.00	0.04	0.39
		617.89%	136.34%	87.99%	75.84%	90.81%	56.19%	83.47%	70.08%	57.50%	32.64%	35.13%	91.60%	40.88%
Xu et al. (2017)	981	0.05	0.02	0.08	0.02	0.02	0.06	0.00	0.00	0.01	0.01	0.27	0.03	0.02
		164.19%	94.29%	94.60%	270.78%	220.87%	44.94%	100.24%	35.48%	87.91%	76.45%	36.15%	46.40%	21.44%
Eter et al. (2017)	2215	0.03	0.10	0.06	0.32	0.11	0.19	0.24	0.02	0.01	0.15	0.00	0.04	0.67
		123.18%	62.90%	56.85%	182.45%	56.37%	39.25%	62.38%	34.43%	53.98%	38.46%	35.16%	35.50%	24.38%
Zhang et al. (2018)	736	0.28	0.66	0.70	0.00	0.54	0.35	0.44	0.56	0.44	0.05	0.64	0.64	0.69
		138.42%	55.22%	41.14%	187.08%	36.40%	49.50%	48.12%	34.45%	34.82%	19.67%	40.29%	45.50%	29.98%
Lei et al. (2019)	997	0.19	0.59	0.71	0.19	0.58	0.39	0.31	0.51	0.66	0.55	0.58	0.64	0.70
		65.04%	35.02%	33.04%	219.41%	60.47%	42.63%	45.29%	46.96%	45.89%	33.86%	51.28%	56.25%	26.27%
Zhang et al. (2020)	93	0.21	0.68	0.70	0.36	0.07	0.40	0.01	0.46	0.61	0.40	0.71	0.69	0.66
		192.46%	112.34%	95.58%	359.93%	110.94%	65.85%	56.06%	39.38%	87.47%	59.73%	43.73%	46.60%	32.71%
Total	12720	0.18	0.43	0.50	0.12	0.11	0.17	0.48	0.68	0.64	0.30	0.27	0.62	0.84
		96.20%	48.79%	44.62%	138.45%	65.75%	47.09%	54.07%	37.30%	44.49%	55.18%	36.36%	36.82%	20.10%
		0.41	0.78	0.83	0.06	0.61	0.44	0.47	0.59	0.64	0.10	0.82	0.80	0.72

When applying the heat transfer correlations to conduct design calculations of heat exchangers, the wall temperature is unknown and essential for determining the heat transfer coefficient. Without the heat transfer coefficient, the thermal resistance and heat transfer rate are unobtainable. Therefore, the performance of the correlations without the wall temperature as input parameters is important. To evaluate the performance of the correlations without inputting wall temperature, an iterative method was adopted (Zhu et al., 2020). Fig. 2 displays the flow chart of the iterative method. During the calculation, the wall temperature was excluded from the input parameters. By assuming the wall temperature, the necessary properties and non-dimensional parameters could be determined, and the Nusselt number and heat transfer coefficient could be accordingly obtained. With the heat transfer coefficient, the new calculated wall temperature could be determined and compared with the assumed wall temperature. The comparison and iteration would be repeated until the error between the assumed and calculated wall temperatures was acceptable.

The summary of MARE and R^2 is shown in Table 4. The results based on each data source and the whole database are displayed detailedly. The proposed correlations in this study showed the best performance with a MARE of 20.10% for the whole database. Moreover, Zhu et al. (2020) also established a database for supercritical heat transfer, including the data for supercritical CO_2, water and R134a, and their correlation was the second-best (MARE=36.36%). The R^2 of the proposed correlations was lower than those of correlations from Jackson and Hall (1979), Jackson (2013), Zhu et al. (2020) and Kim et al. (2008). When the MARE for each data source was concerned, the proposed correlations performed best for the majority. The correlations from Gupta et al. (2013a), Zhu et al. (2020) and Kim et al. (2008) showed the MAREs below 40% for the whole database. Besides, the correlation from Jackson (2013) had the highest R^2 of 0.83 but the MARE was relatively large (44.62%), which indicated that the correlation with higher R^2 cannot always predict the heat transfer better. Compared with the preliminary results with the experimental wall temperature as input parameters, the MARE enlarged and the R^2 decreased for the correlations except for the correlation from Dittus and Boelter (1985) when the iterated wall temperature was adopted. When the iteration of the wall temperature was adopted, it put forward a higher requirement for the heat transfer prediction. The influence of wall temperature iteration on the heat transfer prediction was a research direction for future work.

Table 5 displays the percentage of the data points with an ARE lower than 25% or 50% by applying the correlations. The correlations from Dittus and Boelter (1985), Liao and Zhao (2002) and Kim and Kim (2011a) were excluded due to their MAREs being higher than 60% as Table 4 shows. The proposed correlations can predict 76.33% of the data points with an ARE lower than 25%, which was significantly better than other correlations. Among the correlations from the literature, the correlations from Jackson and Hall (1979), Jackson (2013) and Kim et al. (2008) can predict more than 45% of the data points with the ARE below 25% and more than 70% of the data points with the ARE below 50% as well. The proposed correlations clearly showed better performance for downward flows with $T_b \leq T_{pc}$ and upward flows. For downward flows with $T_b > T_{pc}$, the correlations from Jackson (2013) and Kim and Kim (2010) presented higher percentages with the ARE below 25% than other correlations.

Fig. 3 shows the scatter diagrams that compared the experimental Nusselt number with the calculated results. The correlations from this study, Jackson (2013), Gupta et al. (2013a), Saltanov et al. (2015), Zhu et al. (2020) and Kim et al. (2008) were chosen because they predicted all data points with a MARE below 45% in Table 4. Although the proposed correlations had some dispersed points with large deviations, they still showed the best accuracy and the majority of the data points were within the error bounds of ±50%.

Table 5
Percentage of data points predicted by the correlations with an ARE lower than 25% or 50%.

Conditions	Percentage of data points with a certain range of ARE									
	Downward, $T_b \leq T_{pc}$		Downward, $T_b > T_{pc}$		Upward, $T_b \leq T_{pc}$		Upward, $T_b > T_{pc}$		All data points	
Correlations	ARE ≤ 25%	ARE ≤ 50%	ARE ≤ 25%	ARE ≤ 50%	ARE ≤ 25%	ARE ≤ 50%	ARE ≤ 25%	ARE ≤ 50%	ARE ≤ 25%	ARE ≤ 50%
Jackson and Hall (1979)	51.09%	81.13%	34.36%	78.97%	46.47%	69.79%	46.79%	69.79%	46.66%	70.66%
Jackson (2013)	45.57%	78.56%	74.36%	82.05%	46.45%	71.43%	54.78%	79.32%	49.03%	74.14%
Kim and Kim (2010)	58.54%	84.08%	76.41%	91.28%	25.50%	44.70%	43.97%	72.02%	33.30%	55.17%
Kim and Kim (2011b)	15.79%	24.78%	45.13%	63.59%	32.55%	50.71%	41.84%	72.83%	34.12%	55.07%
Gupta et al. (2013a)	17.07%	60.46%	30.77%	92.82%	33.61%	62.54%	49.67%	83.08%	36.73%	68.30%
Saltanov et al. (2015)	52.37%	71.37%	68.72%	81.03%	30.85%	58.88%	62.30%	87.37%	41.12%	67.54%
Zhang et al. (2018)	15.79%	17.46%	30.77%	63.08%	19.59%	42.08%	26.23%	57.79%	21.28%	44.97%
Zhu et al. (2020)	26.57%	63.80%	9.74%	30.77%	49.91%	77.52%	18.14%	66.56%	39.40%	73.00%
Kim et al. (2008)	39.92%	87.16%	57.44%	77.95%	42.42%	71.95%	53.34%	79.41%	45.37%	74.99%
This study	86.14%	89.86%	57.95%	85.30%	74.90%	86.11%	78.63%	93.11%	76.33%	88.18%

3.3. Prediction of the Nusselt number using the correlations

To verify the capability of the proposed correlations to predict the varying trend of *Nu*, Fig. 4 and Fig. 5 show some comparisons between the experimental and predicted *Nu* for upward and downward flows, respectively. The correlations that had a MARE lower than 45% were applied in this section. Fig. 4(a) shows a set of data from Bae et al. (2010). There was a peak near the pseudo-critical point because the difference between the wall and bulk temperatures reduced to a very low level (Bae et al., 2010). It can be observed that except for the correlations from Gupta et al. (2013a) and Saltanov et al. (2015), the peak was predicted by all the other correlations. All correlations underestimated the peak value of *Nu*, but the proposed correlations outperformed the existing correlations when the T_b was near or higher than the T_{pc}.

Fig. 4(b) depicts a set of data from Zahlan et al. (2015). The experimental *Nu* increased as the T_b increased and a decrease occurred at the end. Only the correlations from Zhu et al. (2020) and this study reflected the decreasing trend at the end. The results of the correlations from Jackson (2013), Zhu et al. (2020) and Kim et al. (2008) were closer to the experimental value at low T_b, however, with the increase of T_b, their deviations became larger than that of the proposed correlation. When T_b increased toward T_{pc}, the specific heat of SCO_2 would increase. Moreover, the peak of average specific heat between bulk and wall temperatures would happen before T_b exactly closed to T_{pc} due to the heating and T_w higher than T_b. The drastic change of average specific heat resulted in the significant variations of heat transfer coefficient and Nusselt number, which was the reason for the increasing deviation of the correlations.

Fig. 4(c) displays a set of data from Jiang (2015). There was a valley of experimental *Nu* near the pseudo-critical point and a peak at T_b lower than T_{pc}. The correlations from this study and Zhu et al. (2020) predicted the variation trend in the highest degree. The model of Zhu et al. (2020) slightly underestimated the *Nu* near the peak and the model in this study underestimated the *Nu* at low T_b. The other correlations cannot represent the valley and peak well.

Fig. 5(a) shows a set of data from Kim and Kim (2011a). Many correlations showed an increasing trend of *Nu*; while only the correlations from this study can present the values and physical trend of the experimental data well. Fig. 5(b) shows a set of data from Li et al. (2010). The increasing trend of the experimental *Nu* was reflected by most of the correlations. But the correlations from this study were obviously the most accurate. Fig. 5(c) depicts a set of data from Liu et al. (2017). The experimental *Nu* had a big decrease near the pseudo-critical point. The decrease of *Nu* was predicted by the correlations from Zhu et al. (2020) and this study. The correlations from this study had the nearest values when T_b was low. Based on the discussion above, it can be concluded that the proposed correlations showed an apparent advantage and were able to accurately predict the SCO_2 heat transfer for upward and downward flows to a higher extent.

3.4. Effects of different parameters

In this section, the effects of different parameters were investigated. Meanwhile, the correlations from Zhu et al. (2020), which had the lowest MARE among the existing correlations as shown in Table 4, and this study were compared.

Fig. 6 shows the influence of the heat flux. It can be seen that *Nu* generally decreased at relatively large T_b when q_w increased. The increase of heat flux would enlarge the radial temperature gradient in the tube, and the thickness of the fluid layer at the pseudo-critical temperature would be reduced (Liu et al., 2016). Thus, the sharp increase of specific heat near the pseudo-critical point had a lower enhancement on the heat transfer, and *Nu* consequently decreased with the increase of heat flux. At q_w of 175 and 250 kW•m^{-2}, the increase of *Nu* at low T_b was slower than that at q_w of 100 kW•m^{-2}, and a decrease of *Nu* could be observed as T_b increased to higher than 32.5°C. In addition, a valley of *Nu* appeared near T_{pc} at q_w of 250 kW•m^{-2}. The increase of *Nu* with the increase of T_b at first was because T_b and T_w were approaching T_{pc}, which led to the decrease of bulk thermal conductivity and the increase of the average specific heat between bulk and wall temperatures. Later, the *Nu* turned to decrease due to the T_w higher than T_{pc} and the decrease of average specific heat. The valley of *Nu* near T_{pc} resulted from the sudden increase of bulk thermal conductivity at the pseudo-critical temperature. The behavior of the above variations was significantly influenced by the heat flux because the heat flux affected the T_w and the average specific heat at the same T_b. With the higher heat flux, the above variation trend of *Nu* would be more obvious. Comparing the predicting performance, the correlation from Zhu et al. (2020) had evident larger deviations when T_b was low at q_w of 100 kW•m^{-2} and T_b was high at q_w of 175 kW•m^{-2}.

Fig. 7 shows the influence of the mass flux. *Nu* increased with the increase of mass flux. When G was 1000 kg•(m^2•s)$^{-1}$, the significant peak of *Nu* happened near T_{pc}. The reason was that the high mass flux led to a low difference between the wall and bulk temperatures. The variation of bulk specific heat near pseudo-critical temperature then dominated the change of HTC. Moreover, under the condition in Fig. 7, the prediction by the correlation from Zhu et al. (2020) was relatively unsatisfactory for both the value and trend.

Fig. 8 shows the influence of the pressure. When T_b was lower than 30°C, the experimental *Nu* was higher at p of 7.5 MPa than that at 9 MPa, which resulted from the decrease of specific heat at higher pressure. But this reduction of *Nu* was slight due to the high ratio of heat flux to mass flux. At high heat flux, the wall temperature in the low-enthalpy region was higher than the pseudo-critical temperature (Lei et al., 2019). Hence, the larger increase of specific heat near the pseudo-critical temperature at 7.5 MPa could only improve *Nu* slightly. As T_b was near T_{pc}, *Nu* at 7.5 MPa had a significant decrease because the thermal conductivity near the pseudo-critical point had a significant increase when the pressure was closer to the critical pressure. The correlation from Zhu et al. (2020) had higher predicting deviations than that of the

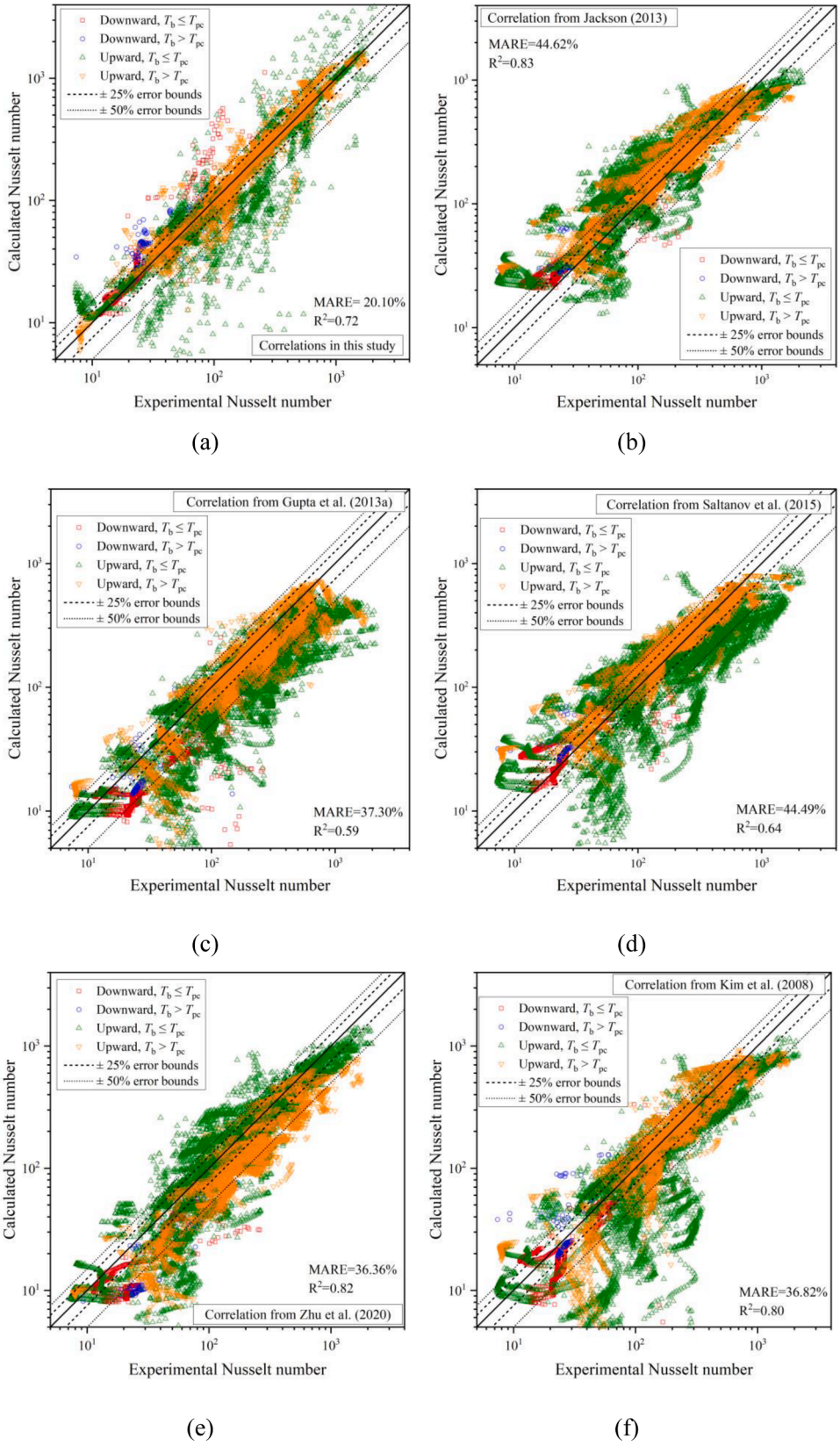

Fig. 3. Scatter diagrams for the comparison between the experimental Nusselt number and the calculated results of the correlations.

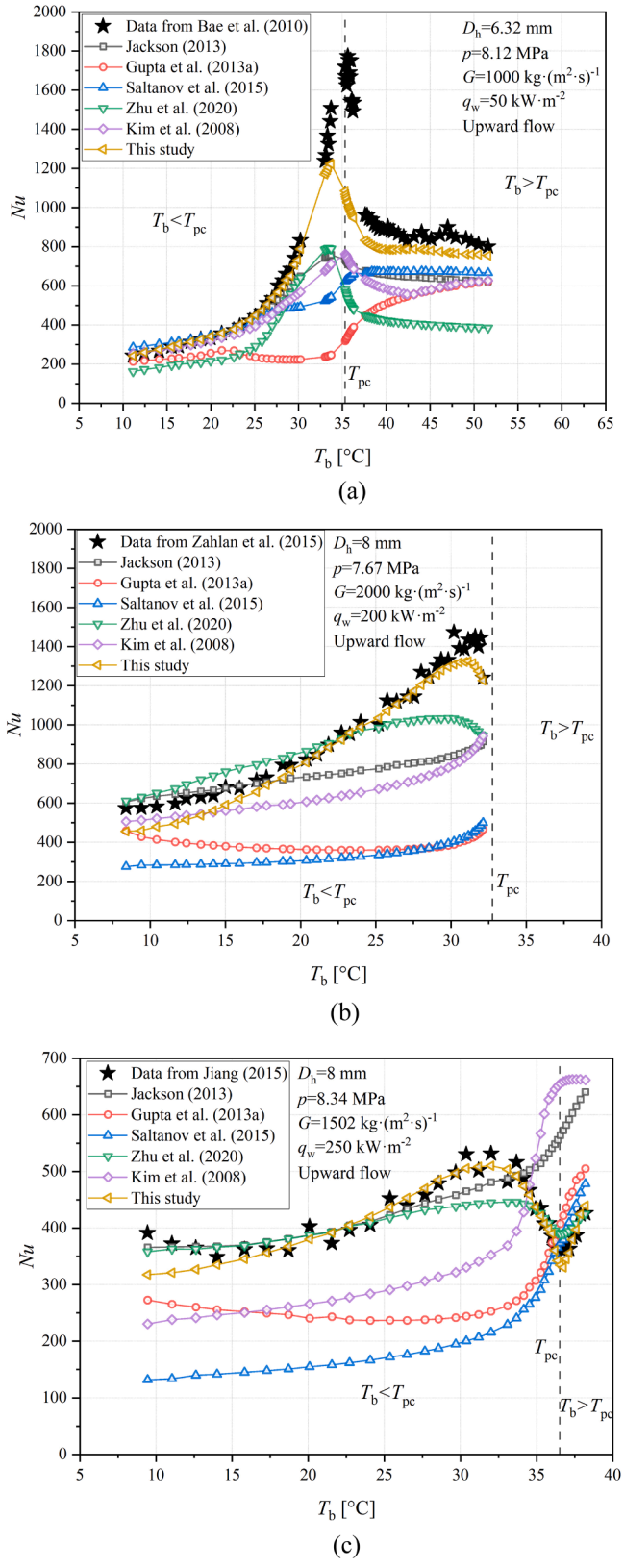

Fig. 4. Comparison of the trend of Nusselt number between the experimental data and the predicted results for upward flows.

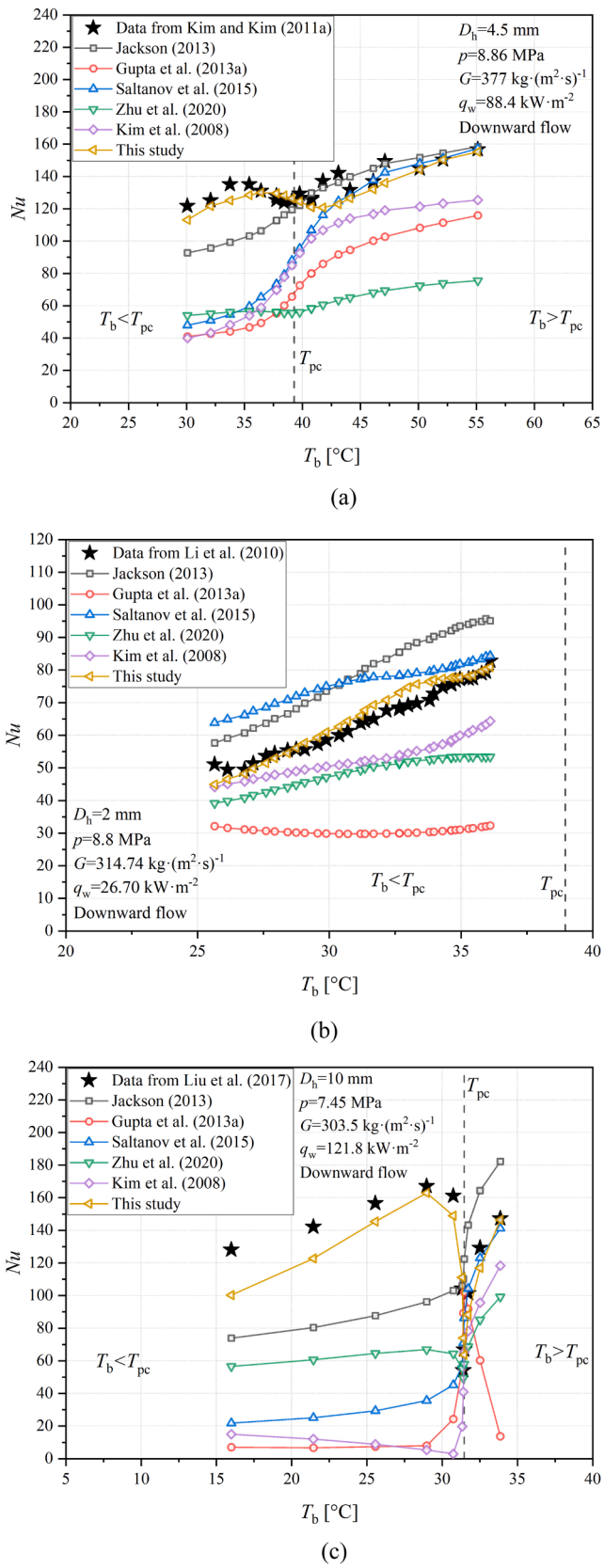

Fig. 5. Comparison of the trend of Nusselt number between the experimental data and the predicted results for downward flows.

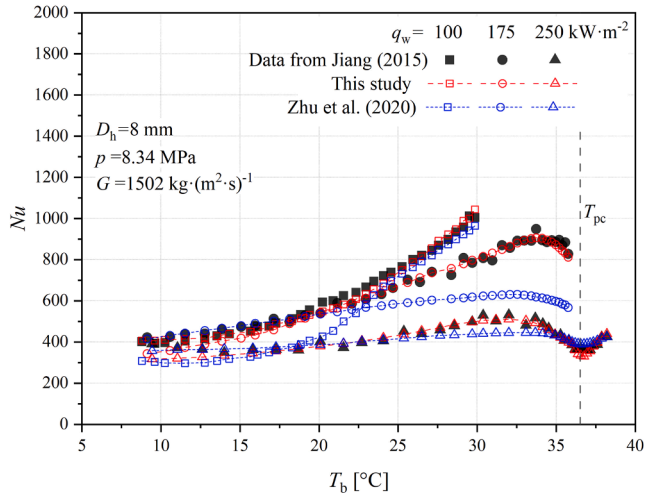

Fig. 6. The measured data (Jiang, 2015) and the results by the correlations from this study and Zhu et al. (2020) for different heat fluxes.

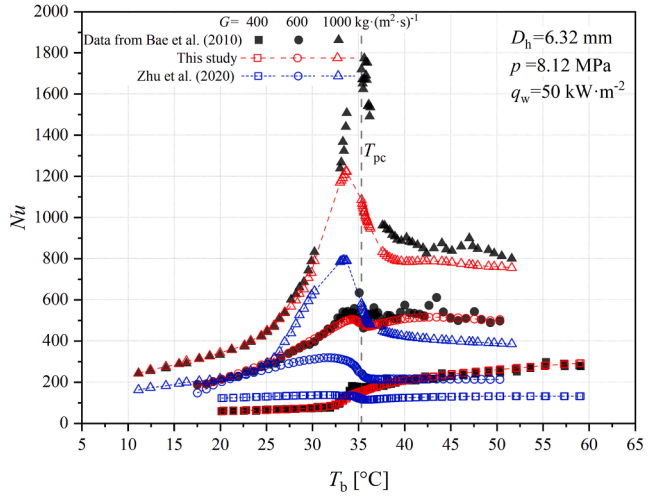

Fig. 7. The measured data (Bae et al., 2010) and the results by the correlations from this study and Zhu et al. (2020) for different mass fluxes.

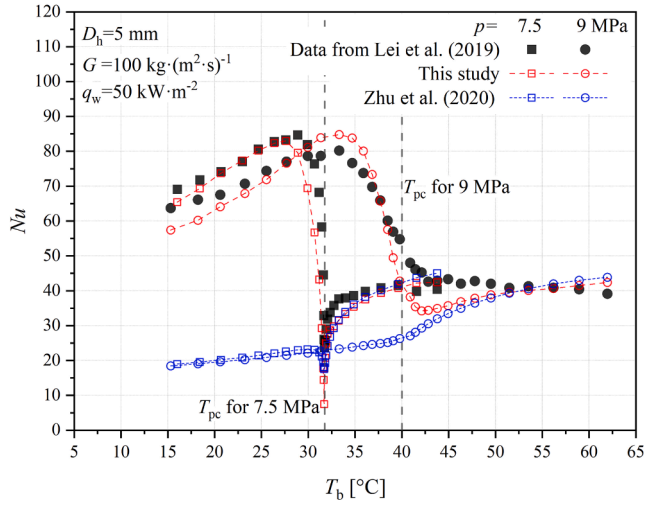

Fig. 8. The measured data (Lei et al., 2019) and the results by the correlations from this study and Zhu et al. (2020) for two pressures.

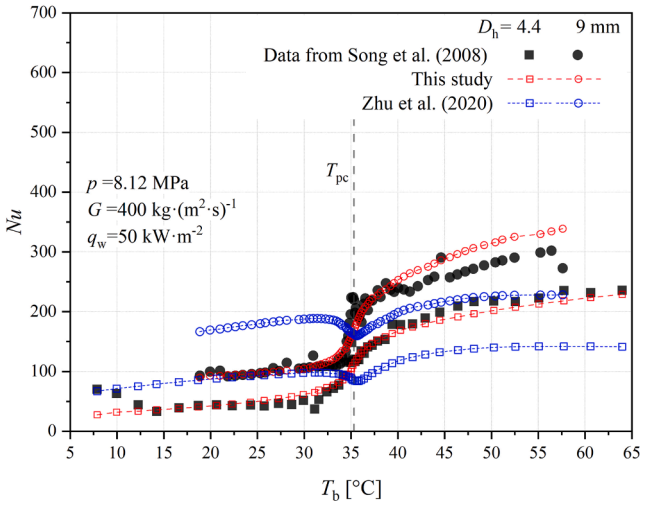

Fig. 9. The measured data (Song et al., 2008) and the results by the correlations from this study and Zhu et al. (2020) for two tube diameters.

correlations in this study when T_b was lower than T_{pc}.

Fig. 9 shows the influence of the tube diameter. Because *Nu* is proportional to the hydraulic diameter, *Nu* was higher when the tube diameter was 9 mm. The variation of *Nu* showed similar patterns with different tube diameters. Compared with the proposed correlations in this study, the prediction by the correlation from Zhu et al. (2020) had a high deviation and the trend was inaccurate as well.

4. Conclusions

In this research, new general heat transfer correlations for SCO_2 heated in vertical tubes for upward and downward flows were developed based on the genetic programming (GP) method. The experimental database contained 12720 data points that covered a wide range of conditions. Some conclusions can be drawn as follows:

(1) Considering Re_b, $\overline{Pr}$, $\frac{\rho_w}{\rho_b}$, $\frac{\mu_w}{\mu_b}$, $\frac{k_w}{k_b}$, $\frac{\overline{c}_p}{c_{p,b}}$, q^+ and *Bu*as the independent variables, the correlations proposed based on the GP method showed superior accuracy. For the entire database, with the iteration of wall temperature, the proposed correlations can predict 76.33% of all data points with the ARE lower than 25% and had a MARE of 20.10%, which was significantly better than all evaluated existing correlations. Besides, the correlation from Jackson (2013) had the highest R^2 of 0.83.

(2) Among the correlations from the literature, only the correlations from Gupta et al. (2013a), Zhu et al. (2020) and Kim et al. (2008) had a MARE lower than 40%. For all the existing correlations, less than 50% of the data points had the ARE below 25%. Furthermore, the correlations from Jackson and Hall (1979), Jackson (2013) and Kim et al. (2008) can predict respectively more than 45% and 70% of the data points with the ARE below 25% and 50%.

(3) The proposed correlations were used to predict the variation trend of *Nu* under different conditions. The results proved that the developed correlations in this study had performance improvement and were able to predict the *Nu* more accurately. Therefore, this study provided general correlations that performed well for a wide range of parameters and can be conveniently applied.

Declaration of Competing Interest

The authors declare that they have no known competing financial interests or personal relationships that could have appeared to influence the work reported in this paper.

Acknowledgement

The authors acknowledge the financial supports from the National Natural Science Foundation of China (No. 51976153), the National Major Science and Technology Project (2017-III-0010-0036), the Foundation for Innovative Research Groups of the National Natural Science Foundation of China (No. 51721004) and the European Union's Horizon 2020 research and innovation programme ('TRI-HP' project, grant number 814888). The first author is grateful for the financial support from the China Scholarship Council and the Department of Energy and Process Engineering, Norwegian University of Science and Technology (NTNU) for his overseas study at NTNU.

References

Bae, Y.Y., Kim, H.Y., Kang, D.J., 2010. Forced and mixed convection heat transfer to supercritical CO_2 vertically flowing in a uniformly-heated circular tube. Experimental Thermal and Fluid Science 34, 1295–1308.

Bae, Y.Y., Kim, H.Y., Yoo, T.H., 2011. Effect of a helical wire on mixed convection heat transfer to carbon dioxide in a vertical circular tube at supercritical pressures. International Journal of Heat and Fluid Flow 32, 340–351.

Cabeza, L.F., de Gracia, A., Fernández, A.I., Farid, M.M., 2017. Supercritical CO_2 as heat transfer fluid: A review. Applied Thermal Engineering 125, 799–810.

Cheng, L., Ribatski, G., Thome, J.R., 2008. Analysis of supercritical CO_2 cooling in macro- and micro-channels. International Journal of Refrigeration 31, 1301–1316.

Cho, B.H., Kim, Y.I., Bae, Y.Y., 2009. Prediction of a Heat Transfer to CO_2 Flowing in an Upward Path at a Supercritical Pressure. Nucl Eng Technol 41, 907–920.

Dittus, F.W., Boelter, L.M.K., 1985. Pioneers in Heat-Transfer - Heat-Transfer in Automobile Radiators of the Tubular Type, 2. Reprinted from University of California Publications in Engineering, pp. 443–461. VolPg1930. International Communications in Heat and Mass Transfer 12, 3-22.

Ehsan, M.M., Guan, Z., Klimenko, A.Y., 2018. A comprehensive review on heat transfer and pressure drop characteristics and correlations with supercritical CO_2 under heating and cooling applications. Renewable and Sustainable Energy Reviews 92, 658–675.

Eter, A., Groeneveld, D., Tavoularis, S., 2017. Convective heat transfer in supercritical flows of CO_2 in tubes with and without flow obstacles. Nuclear Engineering and Design 313, 162–176.

Fan, Y.H., Tang, G.H., Li, X.L., Yang, D.L., Wang, S.Q., 2019. Correlation evaluation on circumferentially average heat transfer for supercritical carbon dioxide in non-uniform heating vertical tubes. Energy 170, 480–496.

Gupta, S., Saltanov, E., Mokry, S.J., Pioro, I., Trevani, L., McGillivray, D., 2013a. Developing empirical heat-transfer correlations for supercritical CO_2 flowing in vertical bare tubes. Nuclear Engineering and Design 261, 116–131.

Gupta, S., Saltanov, E., Pioro, I., 2013b. Heat Transfer Correlation for Supercritical Carbon Dioxide Flowing in Vertical Bare Tubes, 2013 21st International Conference on Nuclear Engineering.

Jackson, J.D., 2013. Fluid flow and convective heat transfer to fluids at supercritical pressure. Nuclear Engineering and Design 264, 24–40.

Jackson, J.D., Hall, W.B., 1979. Forced convection heat transfer to fluids at supercritical pressure. Turbulent forced convection in channels and bundles 2, 563–611.

Jamei, M., Olumegbon, I.A., Karbasi, M., Ahmadianfar, I., Asadi, A., Mosharaf-Dehkordi, M., 2021. On the Thermal Conductivity Assessment of Oil-Based Hybrid Nanofluids using Extended Kalman Filter integrated with feed-forward neural network. International Journal of Heat and Mass Transfer 172, 121159.

Jiang, K., 2015. An Experimental Facility for Studying Heat Transfer in Supercritical Fluids. University of Ottawa.

Jiang, P.X., Liu, B., Zhao, C.R., Luo, F., 2013. Convection heat transfer of supercritical pressure carbon dioxide in a vertical micro tube from transition to turbulent flow regime. International Journal of Heat and Mass Transfer 56, 741–749.

Jiang, P.X., Zhang, Y., Shi, R.F., 2008. Experimental and numerical investigation of convection heat transfer of CO_2 at supercritical pressures in a vertical mini-tube. International Journal of Heat and Mass Transfer 51, 3052–3056.

Kim, D.E., Kim, M.H., 2011a. Experimental investigation of heat transfer in vertical upward and downward supercritical CO_2 flow in a circular tube. International Journal of Heat and Fluid Flow 32, 176–191.

Kim, D.E., Kim, M.H., 2010. Experimental study of the effects of flow acceleration and buoyancy on heat transfer in a supercritical fluid flow in a circular tube. Nuclear Engineering and Design 240, 3336–3349.

Kim, D.E., Kim, M.H., 2011b. Two layer heat transfer model for supercritical fluid flow in a vertical tube. The Journal of Supercritical Fluids 58, 15–25.

Kim, H.Y., Kim, H.R., Kang, D.J., Song, J.H., Bae, Y.Y., 2008. Experimental investigations on heat transfer to CO_2 flowing upward in a narrow annulus at supercritical pressures. Nucl Eng Technol 40, 155–162.

Kim, H.Y., Kim, H., Song, J.H., Cho, B.H., Bae, Y.Y., 2007. Heat Transfer Test in a Vertical Tube Using CO_2 at Supercritical Pressures. Journal of Nuclear Science and Technology 44, 285–293.

Lei, X., Zhang, J., Gou, L., Zhang, Q., Li, H., 2019. Experimental study on convection heat transfer of supercritical CO_2 in small upward channels. Energy 176, 119–130.

Lei, X., Zhang, Q., Zhang, J., Li, H., 2017. Experimental and Numerical Investigation of Convective Heat Transfer of Supercritical Carbon Dioxide at Low Mass Fluxes. Applied Sciences 7, 1260.

Lemmon, E.W., Huber, M.L., McLinden, M.O., 2013. NIST Standard Reference Database 23: Reference Fluid Thermodynamic and Transport Properties-REFPROP, Version 9.1. National Institute of Standards and Technology, Gaithersburg.

Li, Z.H., Jiang, P.X., Zhao, C.R., Zhang, Y., 2010. Experimental investigation of convection heat transfer of CO_2 at supercritical pressures in a vertical circular tube. Experimental Thermal and Fluid Science 34, 1162–1171.

Liao, S.M., Zhao, T.S., 2002. An experimental investigation of convection heat transfer to supercritical carbon dioxide in miniature tubes. International Journal of Heat and Mass Transfer 45, 5025–5034.

Liu, G., Huang, Y., Wang, J., Leung, L.H.K., 2016. Heat transfer of supercritical carbon dioxide flowing in a rectangular circulation loop. Applied Thermal Engineering 98, 39–48.

Liu, S., Huang, Y., Liu, G., Wang, J., Leung, L.K.H., 2017. Improvement of buoyancy and acceleration parameters for forced and mixed convective heat transfer to supercritical fluids flowing in vertical tubes. International Journal of Heat and Mass Transfer 106, 1144–1156.

Rao, N.T., Oumer, A.N., Jamaludin, U.K., 2016. State-of-the-art on flow and heat transfer characteristics of supercritical CO_2 in various channels. The Journal of Supercritical Fluids 116, 132–147.

Sadat Hosseini, A., Hajikarimi, P., Gandomi, M., Moghadas Nejad, F., Gandomi, A.H., 2021. Genetic programming to formulate viscoelastic behavior of modified asphalt binder. Construction and Building Materials 286, 122954.

Saltanov, E., Pioro, I., Mann, D., Gupta, S., Mokry, S., Harvel, G., 2015. Study on Specifics of Forced-Convective Heat Transfer in Supercritical Carbon Dioxide. Journal of Nuclear Engineering and Radiation Science 1, 011008.

Song, J.H., Kim, H.Y., Kim, H., Bae, Y.Y., 2008. Heat transfer characteristics of a supercritical fluid flow in a vertical pipe. The Journal of Supercritical Fluids 44, 164–171.

Sun, F., Xie, G., Song, J., Li, S., Markides, C.N., 2021. Thermal characteristics of in-tube upward supercritical CO_2 flows and a new heat transfer prediction model based on artificial neural networks (ANN). Applied Thermal Engineering 194, 117067.

Xie, J., Liu, D., Yan, H., Xie, G., Boetcher, S.K.S., 2020. A review of heat transfer deterioration of supercritical carbon dioxide flowing in vertical tubes: Heat transfer behaviors, identification methods, critical heat fluxes, and heat transfer correlations. International Journal of Heat and Mass Transfer 149, 119233.

Xu, R.N., Luo, F., Jiang, P.X., 2017. Buoyancy effects on turbulent heat transfer of supercritical CO_2 in a vertical mini-tube based on continuous wall temperature measurements. International Journal of Heat and Mass Transfer 110, 576–586.

Ye, K., Zhang, Y., Yang, L., Zhao, Y., Li, N., Xie, C., 2019. Modeling convective heat transfer of supercritical carbon dioxide using an artificial neural network. Applied Thermal Engineering 150, 686–695.

Zahlan, H., Groeneveld, D., Tavoularis, S., 2015. Measurements of convective heat transfer to vertical upward flows of CO_2 in circular tubes at near-critical and supercritical pressures. Nuclear Engineering and Design 289, 92–107.

Zendehboudi, A., Ye, Z., Hafner, A., Andresen, T., Skaugen, G., 2021. Heat transfer and pressure drop of supercritical CO_2 in brazed plate heat exchangers of the tri-partite gas cooler. International Journal of Heat and Mass Transfer 178, 121641.

Zhang, Q., Li, H., Kong, X., Liu, J., Lei, X., 2018. Special heat transfer characteristics of supercritical CO_2 flowing in a vertically-upward tube with low mass flux. International Journal of Heat and Mass Transfer 122, 469–482.

Zhang, S., Xu, X., Liu, C., Liu, X., Dang, C., 2019. Experimental investigation on the heat transfer characteristics of supercritical CO_2 at various mass flow rates in heated vertical-flow tube. Applied Thermal Engineering 157, 113687.

Zhang, S., Xu, X., Liu, C., Liu, X., Ru, Z., Dang, C., 2020. Experimental and numerical comparison of the heat transfer behaviors and buoyancy effects of supercritical CO_2 in various heating tubes. International Journal of Heat and Mass Transfer 149, 119074.

Zhu, B., Xu, J., Yan, C., Xie, J., 2020. The general supercritical heat transfer correlation for vertical up-flow tubes: K number correlation. International Journal of Heat and Mass Transfer 148, 119080.